Available online at website: https://journal.bcrec.id/index.php/bcrec

Bulletin of Chemical Reaction Engineering & Catalysis, 21 (4) 2026, xxx-xxx

Original Research Article

Deoxygenation of Palm Oil into Hydrocarbon-Rich Fuels over Date Seeds Supported a Bimetallic Ni-Ru Catalyst

Israa A. Jazeel[1], Attared F. Hassan[1], Ali Aldoghachi[2], Faris A. Jasim Al-Doghachi[1,*], Surahim Mohamad[2], Yun Hin Taufiq-Yap[2,3,*]

[1]Chemistry Department, Faculty of Science, University of Basrah, 61004, Basrah, Iraq.
[2]Catalysis Science and Technology Research Center, Faculty of Science, University Putra Malaysia, 43400, UPM Serdang, Selangor, Malaysia.
[3] Institute of Plantation Studies, Universiti Putra Malaysia, 43400, UPM, Serdang, Selangor, Malaysia.

Received: 17th June 2026; Revised: 25th August 2026; Accepted: 26th August 2026
Available online: 5th September 2026; Published regularly: December 2026

Abstract

This study investigates the catalytic deoxygenation of crude palm oil into premium-grade hydrocarbons, employing a series of catalysts, including date seeds (DS), NiO/DS, Ru_2O_3/DS, and bimetallic $NiRu_2O_4$/DS, anchored on a date seed-derived carbon support. The newly synthesized catalysts were characterized using Fourier Transform Infrared (FTIR), NH_3/CO_2-temperature programmed desorption (TPD-NH_3/CO_2), X-ray diffraction (XRD), Brunauer-Emmett-Teller (BET), Field Emission Scanning Electron Microscopy (FE-SEM), Transmission Electron Microscopy (TEM), Thermogravimetric Analysis (TGA), and X-ray photoelectron spectroscopy (XPS) techniques. Structural analysis confirmed that the metal nanoparticles were successfully embedded within the porous matrix of the biomass support, which significantly augmented both the surface area and the density of active sites. At optimized parameters of 350 °C and 40 bar N_2 over a 3 h period, the $NiRu_2O_4$/DS catalyst achieved a maximum hydrocarbon yield of 95%. Detailed chemical profiling of the liquid product showed a high selectivity toward n-Tetradecane (C_{14}) and n-Heptadecane (C_{17}), both critical precursors for bio-jet fuel production. The remarkable performance of the catalyst is fundamentally driven by a synergistic combination of its structural and chemical properties: a higher BET surface area compared to the DS support (4.42 m^2/g), a substantial pore volume of 0.0137 cm^3/g, and a moderate surface basicity of 8534.6 µmol/g. Together, these features facilitate highly efficient deoxygenation pathways via decarboxylation (DCO_2) and decarbonylation (DCO), while effectively suppressing undesirable cracking side reactions. Furthermore, the catalytic system demonstrated exceptional durability, maintaining a robust yield of 88.5% after three consecutive reaction cycles, illustrating the viability of these Ni- and Ru-based materials for renewable aviation energy solutions.

Keywords: Deoxygenation; Impregnation; Date seeds; Palm oil; green diesel

How to Cite: Jazeel, I. A., Hassan, A. F., Aldoghachi, A., Al-Doghachi, F. A. J., Mohamad, S., Yun Hin, T. (2026). Deoxygenation of Palm Oil into Hydrocarbon-Rich Fuels over Date Seeds Supported A Bimetallic Ni-Ru Catalyst. *Bulletin of Chemical Reaction Engineering & Catalysis*, 21 (4), xxx-xxx. (DOI: 10.9767/bcrec.20780)

Permalink/DOI: https://doi.org/10.9767/bcrec.20780

1. Introduction

With the growing recognition that fossil fuel combustion contributes significantly to climate change, increasing attention has been paid to developing sustainable alternatives, including biomass-derived fuels. Biomass is considered a promising substitute for fossil fuels because of its favorable chemical composition [1]. Biofuels are renewable energy sources that represent a potential solution to the increasing global energy demand in both developing and developed countries [2]. Green diesel is a second-generation biofuel that shares the same major structural components as petroleum-based diesel, consisting of alkane hydrocarbons without oxygen atoms [3]. Green diesel is a renewable fuel produced from oils and fats through various conversion processes. In addition to its sustainability and

* Corresponding Authors.
Email: farisj63@gmail.com (F. A. J. Al-Doghachi)'
taufiq@upm.edu.my (T.Y.Y. Hin)

wide availability, green diesel exhibits several favorable fuel properties, including reduced greenhouse gas emissions, a high cetane number resulting from the absence of oxygen-containing compounds in its molecular structure, and a high calorific value [4-6]. Vegetable oils are among the most suitable feedstocks for green diesel production via catalytic deoxygenation. Compared with other biomass resources such as starch and cellulose, which are primarily composed of complex carbohydrates, vegetable oils consist mainly of triglycerides with long-chain aliphatic structures and a relatively low oxygen content. Consequently, they are considered more suitable candidates for biofuel production than other biomass-derived materials. In addition, their wide availability, and physicochemical properties, which are closely comparable to those of conventional petroleum diesel, further enhance their suitability. Among these feedstocks, palm oil has emerged as one of the most extensively studied and promising sources for large-scale green diesel production. The use of palm oil derivatives, such as fatty acid distillates, and waste cooking oils further strengthens its potential as a sustainable feedstock [7]. Green diesel is primarily produced via catalytic deoxygenation (deCO_x) of vegetable oils and free fatty acids under a hydrogen atmosphere. During this process, C16 and C18 fatty acid intermediates undergo complete deoxygenation via decarboxylation, decarbonylation, and hydrodeoxygenation, yielding CO_2, CO, and H_2O as by-products. This conversion results in the formation of paraffinic and olefinic hydrocarbons with shorter carbon chains (C_{15} and C_{17}) relative to their parent fatty acids [8].

Historically, the industrial synthesis of biodiesel has used potassium and sodium hydroxide as the main agents in alkaline catalysis. Although traditional catalysts have chemical advantages such as facile catalysis, rapid kinetics, low cost, easy access, and mild conditions, their operational advantages are severely compromised by their pronounced weakness toward water and free fatty acids (FFAs). This weakness creates unwanted saponification pathways that contribute to soap buildup and increased effluent pollution, thereby elevating the cost of downstream processing and purification [9]. Therefore, these weaknesses negate the benefits and true "greenness" of homogeneous systems. Consequently, overcoming these weaknesses has attracted considerable attention [9]. To this end, a wide range of solid catalysts, including transition-metal oxides, sulfides, phosphides, and carbides, as well as supported noble metals on SiO_2, TiO_2, and Al_2O_3, have been thoroughly evaluated. Noble metal catalysts (Pd, Pt) provide maximum efficiency and green hydrocarbons as products of deoxygenation (DO) transformations, but their prohibitive costs make them economically non-viable [10-12].

Therefore, it is of interest to develop heterogeneous bimetallic catalysts that strike an optimal balance between deoxygenation and mechanical stability. The choice of support materials is crucial as it can enhance the overall efficiency of the active sites by preventing metal leaching and improving thermal stability and metal distribution [13]. Non-noble transition metals, principally nickel, are attracting considerable interest for enhancing catalytic performance and durability in the cleavage of C-C and C-O bonds during deoxygenation. Previous publications suggest that Ni-based catalysts exhibit about 80% selectivity for diesel-range fractions when operated at 390 °C in an inert environment. However, monometallic Ni catalysts suffer from excessive cracking and coking, which negatively affect their structural stability and fuel yield. To address this, the addition of cobalt (Co) to Ni systems was considered; for example, a Co/AC catalyst achieved efficient deoxygenation of palm fatty acid distillate, yielding a hydrocarbon fuel with 91% yield. Interestingly, the Ni-Co bimetallic system exhibits synergistic structural and electronic effects, thereby improving deoxygenation activity at lower temperatures [14]. In catalyst design and development, the greatest importance is placed on the choice of synthesis method. The most significant effects of catalyst synthesis are reflected in the arrangement of atoms within the crystal and in the size and distribution of crystals and particles. Synthesis methods affect the texture of the catalyst's surface and the arrangement of pores to a large degree, which in turn affects overall catalytic activity. Presently, the principal methods of catalyst preparation include wet impregnation, hydrothermal methods, and co-precipitation. Of the three methods, wet impregnation is the most preferred for its ease of use, efficiency, and repeatability at both industrial and laboratory scales. This involves contacting the support with an excess of the precursor solution, followed by controlled thermal drying to remove the solvent [15].

In the present work, a suite of catalysts comprising Date Seeds (DS), NiO/DS, Ru_2O_3/DS, and the bimetallic $NiRu_2O_4$/DS was fabricated via wet impregnation. The physicochemical characteristics and metal-support synergistic effects of the resulting materials were systematically investigated using a comprehensive array of analytical tools. Subsequently, the catalytic efficacy of these systems was examined in the deoxygenation of vegetable oil. A primary objective was the rigorous assessment of catalyst stability and structural

robustness through recyclability experiments across consecutive cycles, thereby evaluating their viability for large-scale industrial deployment.

2. Materials and Method

2.1. Chemical and Materials

This section summarizes the types and suppliers of chemicals and gases, along with their purities, used in this study. All chemicals were used as received from suppliers, without modification or purification. The feedstock used in the deoxygenation process was industrial-grade Crude Palm Oil (CPO), obtained from Selangor, Malaysia. Date seeds (DS) from a local market in Iraq were used as the raw material for the catalyst support. The metallic precursors used for the synthesis of the active metal phases included Nickel(II) nitrate hexahydrate ($Ni(NO_3)_2.6H_2O$) of 98% purity, obtained from Sigma-Aldrich. Anhydrous Ruthenium (III) chloride $RuCl_3$ with 99% purity was obtained from Sigma Aldrich (Merck). Additionally, n-hexane (C_6H_{14}) with 99% purity was obtained from Sisco Research Laboratories Pvt. Ltd. (SRL) and used as a solvent. The gases, Nitrogen (N_2) and Hydrogen (H_2), were of high purity (99.99%).

2.2. Preparation of Date Seed (DS)

The date seeds were washed with boiling distilled water to eliminate impurities and saccharides, then dried for 12 hours at 120 °C. After drying and grinding, the seeds were crushed and sieved to obtain particles smaller than 200 mm. Then, to ensure stability, 200 g of the DS powder was calcined in a furnace at 400 °C for 5 hours under a nitrogen atmosphere at a heating rate of 5 °C/min, after which the material was used as a catalyst support.

2.3. Preparation of the NiO/DS Catalyst

5 wt% NiO was deposited onto DS by dissolving 0.54 gm of $Ni(NO_3)_2.6H_2O$ in 10 mL of methanol, followed by impregnation of the resulting solution onto 30 mL of 95 wt% DS support under continuous stirring for 6 hours. The mixture was dried overnight in an oven at 60 °C. Subsequently, the solid was calcined at 400 °C under nitrogen for 5 hours with a heating rate of 5 °C/min [16]. The Ru_2O_3/DS catalyst was prepared using the same procedures, employing the appropriate weight ratio. For the bimetallic $NiRu_2O_4$/DS catalyst, a precise weight ratio of 90 wt% DS support was dispersed in methyl alcohol. Subsequently, 5 wt% $Ni(NO_3)_2.6H_2O$ and 5 wt% anhydrous $RuCl_3$ were introduced into the DS dispersion. The mixture was stirred for 6 hours, then dried at 60 °C overnight and calcined at 400 °C for 5 hours under an inert nitrogen atmosphere with a heating rate of 5 °C/min.

2.4. Catalyst Characterizations

All synthesized catalysts were analyzed for their physical and chemical properties using several sophisticated methods. The catalysts were characterized for their crystallography and structural properties using powder X-ray diffraction (XRD). XRD analysis of all catalysts was performed using a Shimadzu XRD-6000 diffractometer with a scan speed of 40 °/min and a 2θ range of 2°- 80° to determine the crystalline phases of the supported metals. The average crystallite size of the active metals was determined using the Debye-Scherrer equation. A field-emission scanning electron microscope (FE-SEM) equipped with energy-dispersive X-ray analysis (EDX) (Hitachi S-3400N) was used to study the morphology and elemental composition of the catalysts. To further investigate the chemical states and surface elemental composition of the catalysts, X-ray photoelectron spectroscopy (XPS) was performed using a Thermo Scientific K-Alpha spectrometer with a monochromatic Al Kα X-ray source. The binding energies were calibrated using the C 1s peak at 284.8 eV as an internal standard. This analysis was crucial for determining the oxidation states of the active metals (Ni and Ru) and verifying their interaction with the DS support. Elemental mapping was conducted to confirm the successful loading of 5 wt.% Ru and 5 wt.% Ni on the catalyst. Transmission electron microscopy (TEM; JEOL JEM-2100, Japan) was used and operated at 200 keV.

There are some functional groups on the surface of the date seed support, and their presence was analyzed by Fourier transform infrared spectroscopy (FTIR) before and after modification using a Shimadzu FTIR-8400 (Japan). Ground catalysts and samples were analyzed for specific surface area, pore-size distribution, and pore volume using the Brunauer-Emmett-Teller (BET) method with a Thermo-Finnigan Sorptomatic instrument. Before the analysis, all catalysts were degassed at 150 °C for 12 hours. Adsorption and desorption of N_2 were done using a vacuum chamber at -196 °C. Total acidity and strength of acid sites were measured using NH_3-TPD with a Thermo-Finnigan TPDRO combined with a thermal conductivity detector (TCD). Approximately 0.05 g of catalyst was loaded into a quartz tube and pretreated under a nitrogen atmosphere at 150 °C to remove physically adsorbed moisture. After cooling to room temperature, the sample was exposed to NH_3 gas for 1 h to ensure complete adsorption of ammonia on the acidic sites. Excess NH_3 was then removed by purging with N_2 at a flow rate of 20 mL/min for 35 min. Subsequently, the sample was heated from 50 to 900 °C at a rate of 10 °C/min under a helium flow of 30 mL/ min. The ammonia

desorbed during the temperature-programmed desorption process was continuously monitored using a thermal conductivity detector (TCD).

Final analyses were conducted with the TGA 1000i instrument (Instrument Specialists Inc., USA) for Thermogravimetric Analysis (TGA) to assess the thermal stability of the catalysts. Since the deoxygenation reactions occur at higher temperatures (> 300 °C), it was important to maintain the thermal integrity of the date seed-based catalyst. The sample was heated from 25 °C to 900 °C at a heating rate of 10 °C/min while nitrogen gas was flowing at 40 mL/min. The weight loss was plotted against the increase in temperature.

2.5. Catalytic Deoxygenation of Palm Oil

To deoxygenate palm oil while keeping excellent temperature and stirring control, a 250 mL semi-batch reactor system with a TOPO MS-DMS mixing mantle was employed. The common method entails mixing 9.8 g of palm oil with 0.2 g of the manufactured Ni-Ru/DS catalyst. The reaction was maintained at a constant temperature of 350 °C for three hours. Continuous mixing was carried out at 400 rpm (equivalent to 40 on the ×10 rpm scale) to minimize mass-transfer resistance and ensure uniform dispersion of the catalyst throughout the oil phase. The volatile compounds evolved during the reaction were condensed through an external water-cooled condensation system maintained at 15 °C. The condensed products were then transferred into a receiving flask for subsequent characterization and analysis.

The oxygen-free liquid products (green diesel) were further examined using gas chromatography-mass spectrometry (GC-MS) and gas chromatography with a flame ionization detector (GC-FID). These methods were used to determine the quantity and chemical composition of the generated hydrocarbons.

2.6. Product Characterization

To identify and correlate the peaks during analytical analysis of the liquid products, a standard hydrocarbon mixture of C_8-C_{35} alkanes and alkenes was used. The deoxygenated liquid products were characterized using a Shimadzu QP2010 Plus GC–MS system equipped with a Zebron ZB-5MS capillary column (30 m × 0.25 mm × 0.25 µm) and operated in splitless injection mode. Prior to analysis, the samples were diluted to 100 ppm using high-purity n-hexane (>98%). The resulting chromatographic and mass spectral data were used to identify and quantify the organic constituents. The equation assigned to it was used to calculate liquid deoxygenation product selectivity:

$$S_{\text{product}}\ \% = \frac{Cy}{\sum ny} \times\ 100\% \quad (1)$$

such that S_{product}% represents the percentage selectivity of products, while Cy denotes the individual peak area of the specific organic compound, and $\sum ny$ refers to the total area of the organic products identified in the liquid, thereby quantifying the relative distribution of each compound within the mixture phase. A Gas Chromatograph with a Flame Ionization Detector (GC-FID) system (Shimadzu GC-14B) was used for quantitative analysis. The liquid product from the deoxygenation phase was diluted with n-hexane as the internal standard. 1 µL of the diluted liquid was injected into the system using an HP-5 capillary column (30 m × 0.32 mm. The detector temperature was maintained at 300 °C throughout the analysis. The hydrocarbon yield, kerosene-range fraction, and bio-jet fuel (BJF) selectivity were subsequently calculated using Equations (2), (3), and (4), respectively.

$$Hydrocarbon\ yield\ (\%) = \frac{\sum Area\ of\ alkane(C8-C20)+\sum Areaof\ alkene(C8-C20)}{\sum Area\ of\ the\ product} \times 100\% \quad (2)$$

$$Kerosene\ yield\ (\%) = \frac{\sum Area\ of\ alkane\ (C8-C16)+\sum Area\ of\ alkene(C8-C16)}{\sum Area\ of\ the\ product} \times 100\% \quad (3)$$

$$BJF\ selectivity\ (\%) = \frac{\sum Total\ area\ of\ alkane\ \&\ alkene\ (C11+C13+C15)}{\sum Area\ of\ alkane(C8-C20)+\sum Area\ of\ alkene\ (C8-C20)} \times\ 100\% \quad (4)$$

Following the catalyst screening phase, the synthesized catalyst with the highest performance was chosen for the parametric study using the OVAT technique. It achieved the highest hydrocarbon yield (HC%) with high selectivity towards Green Diesel in the deoxygenation reaction. To determine the ideal operating parameters, the reaction time was varied from two to six hours, while reaction temperatures were tested at 270, 300, 350, and 370 °C. The liquid products from the optimization study were analyzed by GC-FID to determine the conditions that achieved the maximum hydrocarbon content and the highest selectivity for Green Diesel.

2.7. Reusability and Stability of the Catalyst

Further examination of the reusability and stability of the synthesized catalyst was done under the optimized reaction parameters. Reusability studies were conducted using spent catalysts that were recovered after each deoxygenation (DO) cycle. After deoxygenation,

the spent catalyst was separated from the liquid product and washed several times using n-hexane to eliminate any adsorbed organic material. The catalyst was dried and heated at 100 °C for 4 hours before being used for the next reaction. The results for each cycle were analyzed using the hydrocarbon yield, the kerosene fraction, and the product selectivity as described in Eqs. (2), (3), and (4), respectively. The properties of spent catalysts were analyzed using TGA, TEM, and XRD, and the deoxygenated liquid from each cycle was analyzed using GC-FID.

3. Results and Discussion

3.1. Structural and Textural Properties of the Catalysts

The crystalline structure and phase composition of the prepared catalysts were investigated using XRD analysis over a 2θ range of 2-80°. Peak assignment was performed using the International Centre for Diffraction Data (ICDD). The obtained patterns are illustrated in Figure 1. The XRD pattern of the raw Date Seed (DS) support exhibits a broad diffraction feature centred at approximately 2θ = 23.5°, indexed to the (0 0 2) planes of disordered graphitic carbon (ICDD 41-1487) [17], while the absence of sharp peaks confirms the amorphous nature of the support. The NiO/DS catalyst shows sharp, intense peaks, primarily at 2θ = 37.44°, 43.3°, and 75.374°, corresponding to the (1 1 1), (2 0 0), and (3 1 1) planes, indicating the presence the face-centered cubic FCC structure of NiO (ICDD 04-0787) [6]. The XRD profile of the Ru_2O_3/DS catalyst exhibited only faint diffraction peaks with relatively low intensities at 2θ = 42.4° and 44.37°, corresponding to the (0 0 2) and (1 0 1) planes. This reflection can be attributed to crystalline ruthenium oxide species with the Ru_2O_3 phase (ICDD 00-002-1365). The relatively low intensity of these peaks suggests a high dispersion of Ru oxide species across the support surface, together with small crystallite dimensions and/or poor crystallinity. Such characteristics limit the detectability of the Ru_2O_3 phase by X-ray diffraction, resulting in the observed weak diffraction signals [18].

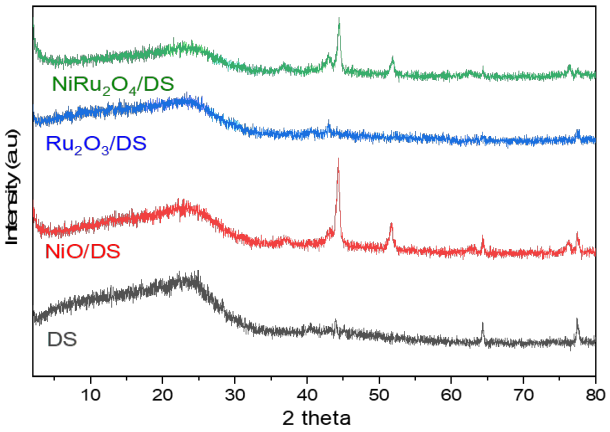

Figure 1. XRD patterns for DS, NiO/DS, Ru_2O_3/DS, and $NiRu_2O_4$/DS.

Meanwhile, the bimetallic $NiRu_2O_4$/DS catalyst exhibited distinctive diffraction peaks at 2θ = 37.093° (1 1 1), 43.096° (2 0 0), and 51.596° (2 0 0), which are attributed to the face-centred cubic (FCC) structure of NiO (reference code 04-0787). Additionally, a specific peak observed at 2θ = 44.37° (2 0 0) was assigned to the presence of Ru_2O_3 species (ICDD 00-002-1365), confirming the successful integration of both active phases within the bimetallic catalytic architecture. The Debye-Scherrer equation [15] was applied to determine the crystal size of catalysts from the diffraction of the highest peaks in the XRD patterns. The observed crystal sizes were 17.41 nm, 17.50 nm, 13.34 nm, and 20.21 nm, for the following catalysts: DS, NiO/DS, and $NiRu_2O_4$/DS, respectively. The fine crystallite size observed for the bimetallic catalyst (20.21 nm) indicates uniform metal distribution, thereby increasing the number of exposed active centers and enhancing catalytic efficiency.

The surface morphology and structural evolution of the synthesized samples were evaluated using FE-SEM, revealing distinct transitions among the materials. The raw data seeds (DS) [Figure 2-A] initially exhibit an irregular, amorphous, and highly heterogeneous morphology composed of sharp-edged flakes and sub-micron blocks aggregated into larger clusters, confirming a porous matrix, suitable for catalyst support. Upon modification, the NiO/DS catalyst displays a distinct multi-phasic structure. The underlying carbonaceous sheets become heavily decorated with a dense, uniform distribution of granular NiO/DS nanoparticles and coral-like clusters driven by active surface anchoring sites. In contrast, the Ru_2O_3/DS composite shows dense polymeric sheets interwoven with irregular carbon blocks, acting as a robust substrate finely embedded with sub-micron, spherical grain-like clusters and ultra-fine Ru_2O_3/DS particulates. Ultimately, the bimetallic $NiRu_2O_4$/DS composite reveals a synergistic structural modification. Large, smooth underlying carbon sheets are extensively covered by a highly dispersed network of fragmented flakes, nanoparticles, and porous aggregates, indicating the successful co-deposition of both Ni and Ru oxide phases, which effectively suppresses severe self-agglomeration and maximizes the number of exposed catalytically active sites.

Using FTIR spectroscopy, the surface chemical functionality of the synthesized catalysts and the unprocessed Date Seed (DS) support was examined in the spectral region of 4000-400 cm^{-1}.

All samples' spectra display a wide absorption band between 3400 and 3600 cm^{-1}, attributed to O-H stretching vibrations of adsorbed moisture and residual phenolic groups. The continuous band at 1604 cm^{-1} corresponds to aromatic C=C skeletal vibrations, confirming the structural stability of the carbonaceous framework after calcination at 400 °C [17]. Except for the DS support, all catalysts exhibited distinctive bands in the 400-650 cm^{-1} region, which are attributed to metal-oxide (Ni-O and Ru-O) stretching and bending vibration modes [19-21]. This spectroscopic behaviour suggests the development of a stable bimetallic oxide interface on the treated carbon substrate. The FTIR data are consistent with the XRD and FE-SEM-EDX analyses, demonstrating that the calcination procedure successfully anchored the active metal oxide phases and aided in the formation of an active catalytic surface.

To evaluate the textural characteristics of the prepared catalysts (DS, NiO/DS, Ru_2O_3/DS, and $NiRu_2O_4$/DS), N_2 adsorption-desorption isotherms were analyzed to determine their BET surface area, pore volume, and pore diameter (see Table 2). All samples exhibited a pattern similar to type IV isotherms according to the International Union of Pure and Applied Chemistry (IUPAC) classification, confirming the predominant presence of a mesoporous framework. Moreover, the noticeable increase in nitrogen uptake at elevated relative pressures ($P/P_0 \approx 0.8$-1.0) suggests capillary condensation within the pore channels, confirming an interconnected network of mesopores and macropores (see Figure 4). Based on the results summarized in Table 2, the bimetallic $NiRu_2O_4$/DS exhibited the highest surface area of 4.4204 m^2/g compared with the DS-support (1.7541 m^2/g), together with a pore diameter of 6.4284 nm and a pore volume of 0.013734 cm^3/g, suggesting uniform metal dispersion and improved accessibility of catalytic sites. The obtained pore size of 6.4284 nm is well situated in the mesoporous range, making it favourable for the diffusion and adsorption of fatty acid triglyceride molecules (kinetic

Table 1. The average elemental content levels were obtained.

Catalyst	C (wt%)	O (wt%)	Ni (wt%)	Ru (wt%)	other material (wt%)
Date seed (DS)	83.72	12.63	-	-	1.91
NiO/DS	73.95	16.78	7.14	-	1.53
Ru_2O_3/DS	83.29	15.73	-	1.21	-
$NiRu_2O_4$/DS	72.22	25.36	1.71	0.71	-

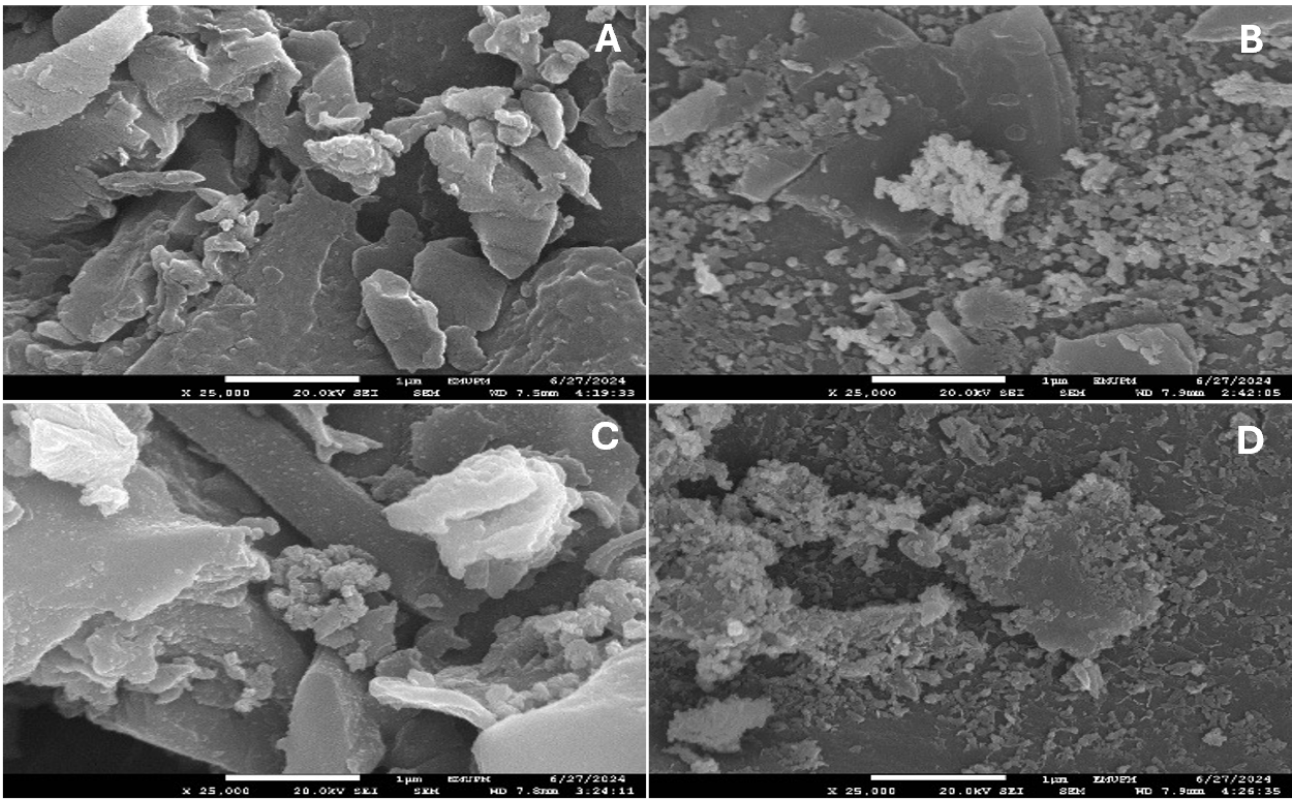

Figure 2. FESEM image of catalysts A) DS, B) NiO/DS, C) Ru_2O_3/DS, D) $NiRu_2O_4$/DS.

diameter for fatty acid chains ~ 2-3 nm). The synergistic effect of elevated surface area and suitable pore size enhances reactant and product diffusion, thereby increasing catalytic efficiency [23]. In contrast, the Ru_2O_3/DS catalyst exhibited a lower surface area of 1.9080 m²/g and a smaller pore volume, which may be attributed to the accumulation or agglomeration of ruthenium particles on the support surface, partially blocking the pores. Meanwhile, the raw DS exhibited the lowest surface area, indicating that metal incorporation played an important role in developing the material's surface texture. It was also observed that the metal-loaded catalysts exhibited larger pore diameters than the untreated support, suggesting that impregnation and calcination promoted the formation of more developed porous channels. Overall, the improvement in the textural properties, particularly for the $NiRu_2O_4$/DS catalyst, explains its superior catalytic performance and higher selectivity toward long-chain hydrocarbons (C_{15}+C_{17}) during the deoxygenation of palm oil. The NiO/DS catalyst showed a surface area of 4.3780 m²/g, which is significantly higher than that of DS (1.754 m²/g), indicating that the incorporation of NiO contributed to the development of the surface structure and generation of additional active sites. In addition, the catalyst exhibited an increase in pore volume to 0.012829 cm³/g, thereby enhancing mass transfer and molecular diffusion within the pore channels during the deoxygenation (DO) reaction.

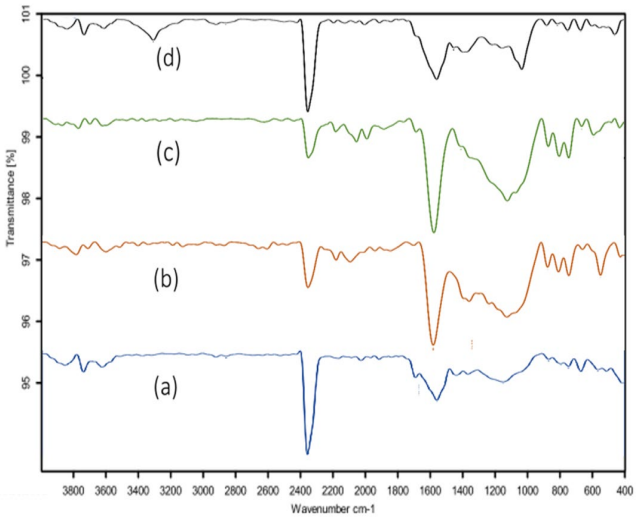

Figure 3. FTIR spectra of a) DS, b) NiO/DS, c) Ru_2O_3/DS, and d) $NiRu_2O_4$/DS.

Using thermogravimetric analysis (TGA), the thermal stability and breakdown behaviour of the produced catalysts (DS, NiO/DS, RuO_2/DS, and $NiRu_2O_4$/DS) were assessed between 25 and 1000 °C under a nitrogen environment. Every TGA thermogram, as shown in Figure 5, displayed a multi-step weight loss pattern corresponding to various thermal occurrences. The first phase, which occurred at temperatures below 150 °C, with weight loss of 2-5%, attributed to the evaporation of water and moisture

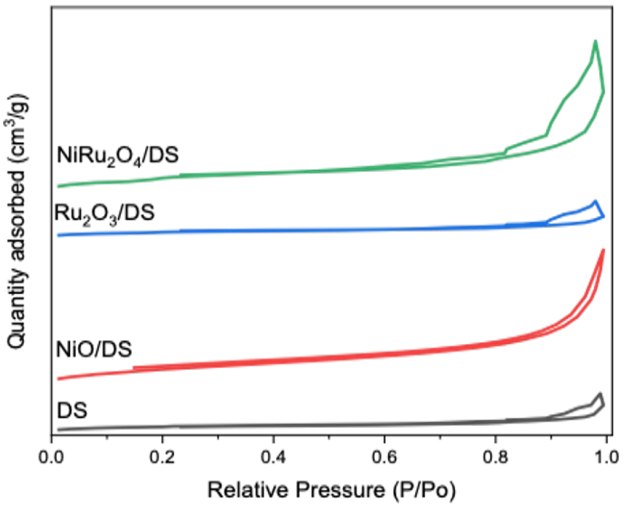

Figure 4. Isotherm linear plot for the new catalyst.

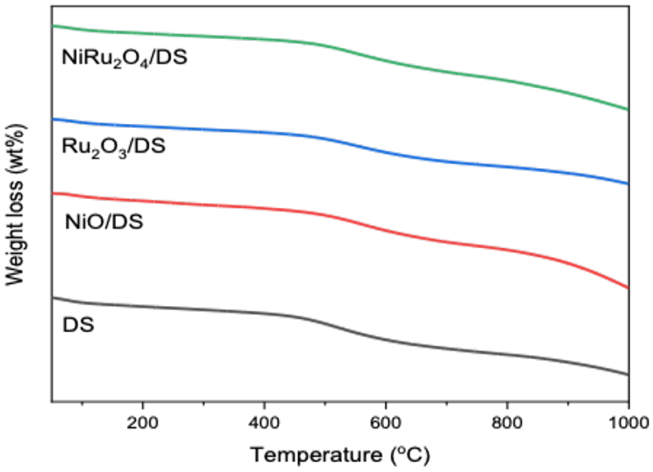

Figure 5. TGA analysis for new catalysts.

Table 2. N_2-adsorption/desorption analysis.

Catalyst	Surface area (m²/g)	Pore size diameter (nm)	Pore volume (cm³/g)
DS (Date seeds)	1.7541	4.4220	0.003368
NiO/DS	4.3780	6.0928	0.012829
Ru_2O_3/DS	1.9080	4.2092	0.003180
$NiRu_2O_4$/DS	4.4204	6.4284	0.013734

physically adsorbed on the surface of the Date seeds (DS) support, as well as to moisture retained within its mesoporous structure. the second weight loss stage occurred between 250 and 600 °C, during which the carbonaceous matrix thermally degraded and carbonized. Compared with the raw support, all metal-loaded catalysts, notably the bimetallic $NiRu_2O_4$/DS, exhibited a clear shift of the decomposition peaks toward higher temperatures. These behaviour suggest that the presence of NiO and Ru_2O_3 nanoparticles provides thermal shielding, enhancing the structural stability of the catalysts. The weight-loss curves plateaued at temperatures above 600 °C, indicating that inorganic residues were formed. Quantitative evidence for the successful impregnation of thermally stable and nonvolatile nickel and ruthenium oxides was demonstrated by the bimetallic catalyst $NiRu_2O_4$/DS, which retained the highest remaining mass at 1000 °C across all samples. These findings, collectively, demonstrate that the $NiRu_2O_4$/DS catalyst exhibits outstanding thermal stability up to 450 °C, rendering it ideal for a wide range of catalytic applications and highlighting the positive synergistic impact of the bimetallic oxides on the Date Seeds support. The thermal stability and degradation resistance of the catalysts followed the descending order: $NiRu_2O_4$/DS > Ru_2O_3/DS > NiO/DS > DS, with corresponding residual masses of 79.5%, 64.8%, 58.2%, and 41.7% at 1000 °C, respectively. These values indicate that all synthesized catalysts exhibit high thermal stability; however, the bimetallic $NiRu_2O_4$/DS demonstrates the superior resistance to thermal decomposition. This confirms that the synergistic integration of Ni and Ru nanoparticles significantly enhances the structural integrity and thermal endurance of carbon support.

The successful formation of the catalyst nanostructures was evidenced by the internal morphology, crystallinity, and particle size distribution of the catalysts, as measured by Transmission Electron Microscopy (TEM), as depicted in Figure 6. The TEM images of the unmodified Date Stone (DS) reveal a predominantly porous, amorphous carbon matrix with clear channels that serve as ideal anchorage sites for metal nanoparticles with average particle sizes of 7-11 nm. The images for NiO/DS and Ru_2O_4/DS demonstrate that, upon the addition of metals, dark, spherical-like nanoparticles are uniformly dispersed along the carbon support with an average particle size of 6 to 68 nm for the NiO/DS and from 6 to 10 nm for the Ru_2O_4/DS catalyst. The bimetallic $NiRu_2O_4$/DS catalyst is notable for a highly uniform, non-agglomerated distribution of nanoparticles with particle sizes averaging between 5-10 nm, suggesting that the applied synthesis strategy successfully constrained the metallic phases to a specific size. Moreover, high-

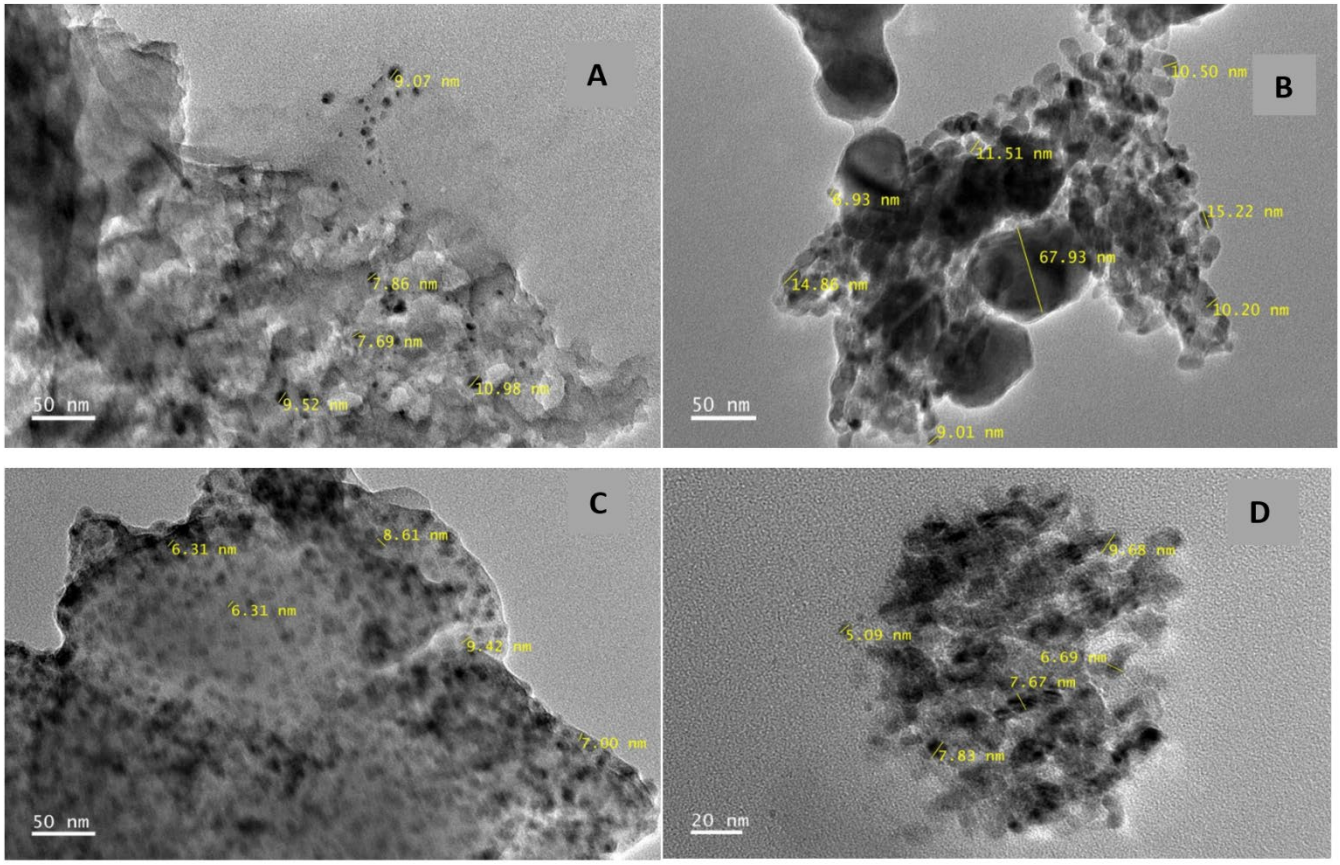

Figure 6. TEM image of catalysts: A) DS, B) NiO/DS, C) Ru_2O_3/DS, D) $NiRu_2O_4$/DS.

magnification views of the $NiRu_2O_4$/DS show well-defined porous fringes, corresponding to the gaps between adjacent planes of the crystal lattice, further confirming the crystallinity of the $NiRu_2O_4$ phase and its alignment with the XRD diffraction pattern. As seen in the TEM micrographs, the close contact between the bimetallic nanoparticles and the porous DS framework accounts for the increased surface area and improved thermal stability, as evidenced by the BET and TGA analyses, respectively. This structural arrangement increases the density of active sites, which is essential for the excellent catalytic activity of the bimetallic system.

The acidic and basic properties of the synthesized catalysts were evaluated using NH_3-TPD and CO_2-TPD analyses. Based on the desorption temperatures, the acid/base sites were categorized as weak below 250 °C, moderate between 250 and 500 °C, and strong above 500 °C [23]. The acidity profiles are presented in Figure 7 and Table 3. Catalyst acidity plays a crucial role in the deoxygenation of vegetable oils by activating oxygen-containing compounds and facilitating C-O bond cleavage, thereby enhancing oxygen removal and converting oils into hydrocarbons suitable for green diesel production. Acidic sites also improve the adsorption of reactants onto the catalyst surface and increase reaction efficiency. Moderate to strong acidity is considered important for promoting the formation of diesel-range hydrocarbons, whereas excessively high acidity may lead to excessive cracking and coke formation [8].

All catalysts exhibited dominant, strongly acidic sites, as evidenced by the intense NH_3 desorption peaks observed at temperatures above 550 °C. These acidic sites primarily arose from the intrinsic acidity of the date seed-derived support (DS), with contributions from chemisorbed ammonia species. Furthermore, the desorption peak appearing above 500 °C may partially result from the formation of NO_x species generated through the interaction between ammonia and surface oxygen species [24].

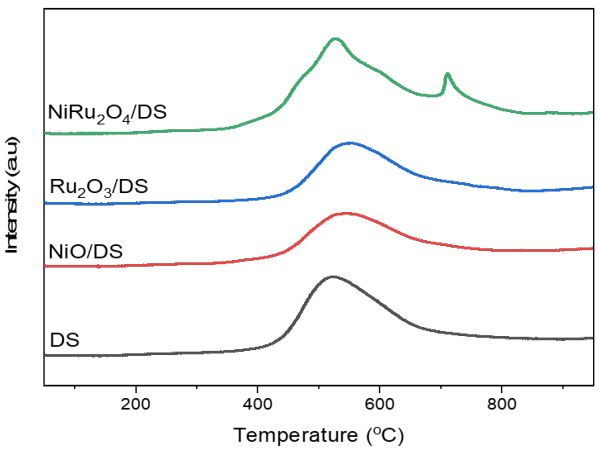

Figure 7. TPD-NH_3 acidity profiles of the prepared catalysts.

Among the prepared catalysts, the $NiRu_2O_4$/DS catalyst exhibited the highest acidity value of (2334.8 µmol/g), whereas DS showed the lowest acidity strength of (1022.5 µmol/g). The significant increase in acidity from 1022.5 µmol/g for DS to 2334.8 µmol/g for NiRu/DS can be attributed to the incorporation of nickel and ruthenium oxide species onto the porous carbonaceous support. Metal oxides are known to introduce additional acidic sites through surface hydroxyl groups and coordinatively unsaturated metal ions. The NiO and RuOx phases provide abundant Lewis's acid sites due to the electron-deficient nature of Ni^{2+} and Ru cations, which can accept electron pairs from adsorbed molecules. Furthermore, the interaction between nickel oxide and ruthenium oxide generates a synergistic effect that enhances charge polarization at the catalyst surface, leading to stronger acidity [22]. The high dispersion of the mixed-oxide nanoparticles on the DS support, as observed by TEM, increases the accessibility of these acidic centers. In addition, the strong interaction between the oxide phases and the oxygen-containing functional groups of the DS support may create new surface acid sites and increase the overall acid density, which is beneficial for activating C-O bonds and facilitating DCO_2/DCO reactions, while minimizing secondary cracking and condensation reactions [8]. The acidity of the catalysts increased in the following order: The total acidity, representing the amount of desorbed NH_3, followed a decreasing order: $NiRu_2O_4$/DS > RuO_2/DS > NiO/DS > DS.

The surface basicity and active-site distribution of the synthesized catalysts were evaluated using TPD-CO_2, with the results summarized in Table 4 and Figure 8. Catalyst basicity plays a crucial role in deoxygenation (DO) reactions; the presence of basic sites helps activate the carboxylic functionality of fatty acids and promotes oxygen removal via DCO_2 and DCO routes. Consequently, moderate basicity is optimal for the efficient and stable conversion of vegetable oils into green diesel [8,25].

Table 3. Surface acidity and NH_3 desorption parameters of the synthesized catalysts.

Catalyst	NH_3- desorption temperature (°C)	Amount of NH_3-desorbed (µmol/g)
Date Seeds (DS)	585	1022.5
NiO/DS	638	1245.3
Ru_2O_3/DS	645	1856.7
$NiRu_2O_4$/DS	622	2334.8

TPD-CO_2 measurements were performed to assess the surface basicity of the prepared catalysts and to investigate the interaction behavior of CO_2 molecules with the catalyst surfaces. As observed, all catalysts exhibited desorption peaks at high temperatures above 500 °C, indicating the presence of strong basic sites and strong interactions between CO_2 and the catalyst surface. According to Wierzbicki *et al.* [25], weak, moderate, and strong basic sites are associated with surface hydroxyl groups (OH^-), Lewis's acid-base pairs, and low-coordination O^{2-} species, respectively. Among the catalysts studied, $NiRu_2O_4$/DS exhibits the highest surface basicity (8534.6 µmol/g), as summarized in Table 4. This enhancement can be attributed to NiO's role in generating new basic oxygen sites on the catalyst surface. The surface oxygen ions (O^{2-}) associated with NiO act as Lewis basic sites that effectively adsorb CO_2, thereby increasing the amount of adsorbed CO_2 and enhancing the catalyst's overall basicity [26]. Furthermore, Ruthenium oxide improved the dispersion of the active species on the support surface and strengthened the synergistic interaction between Ni and the carbonaceous support. This synergistic effect increased the number of active surface sites available for CO_2 adsorption and enhanced the density of basic sites [27]. In contrast, NiO/DS exhibits the lowest surface basicity, even lower than that of the pristine DS support. This reduction is mainly due to the partial blockage of the carbon surface's inherent basic pores and active sites by the deposition of NiO particles. The data reveal that the total amount of desorbed CO_2 decreases in the order: $NiRu_2O_4$/DS > Ru_2O_3/DS > DS > NiO/DS.

Surface elemental distribution and oxidation states of the $NiRu_2O4$/DS-derived catalyst were investigated using X-ray photoelectron spectroscopy (XPS). This technique is essential for elucidating the chemical environment and electronic interactions between the active phase and the date-seed-derived carbon support (DS). The binding energy distributions for Ni, Ru, and O provide definitive evidence regarding the surface chemistry and oxide formation, as illustrated in Figure 9. The Ni 2p spectrum (Figure 9A) displays a predominant sharp peak in the range of 853.5-855.2 eV, which is characteristic of Ni^{2+} ions within the NiO lattice. This primary peak is accompanied by a distinct shake-up satellite feature near 861-865 eV, resulting from complex electronic transitions that confirm NiO as the predominant surface oxide. Furthermore, the well-resolved $2p_{3/2}$ and $2p_{1/2}$ doublets at higher binding energies (above 870 eV) exhibit significant spin-orbit splitting. This energetic separation indicates strong chemical stability and robust anchoring of the Ni ions to the carbonaceous matrix [28,29]. Regarding the Ru 3d spectrum (Figure 9B), deconvolution reveals a primary doublet with a binding energy for Ru 3d5/2 at approximately 281.8-282.5 eV, which is attributed to Ru^{3+} ions, confirming the presence of Ru_2O_3 within the catalyst structure. The overlap observed near 284.6 eV corresponds to the C 1s signal from the DS support, while the components at higher binding energies (286.5-288.0 eV) suggest the formation of Ru-O-C bonds. These interactions facilitate electronic coupling between the ruthenium species and the carbon support, enhancing the synergistic effect for efficient deoxygenation [28]. Regarding the O 1s spectrum (Figure 9C), deconvolution was employed to resolve two distinct oxygen environments. The first peak, assigned to lattice oxygen OL, appears at 529.8-530.1 eV and corresponds to the metal-oxygen bonds in NiO. The second peak, situated around 531.8-532.5 eV, is attributed to surface-adsorbed or chemisorbed oxygen OS, representing hydroxyl groups (-OH) or oxygen species associated with the DS support. These findings highlight a strong synergistic interaction and stable chemical bonding between the active NiO phase and the carbonized date seed surface [29].

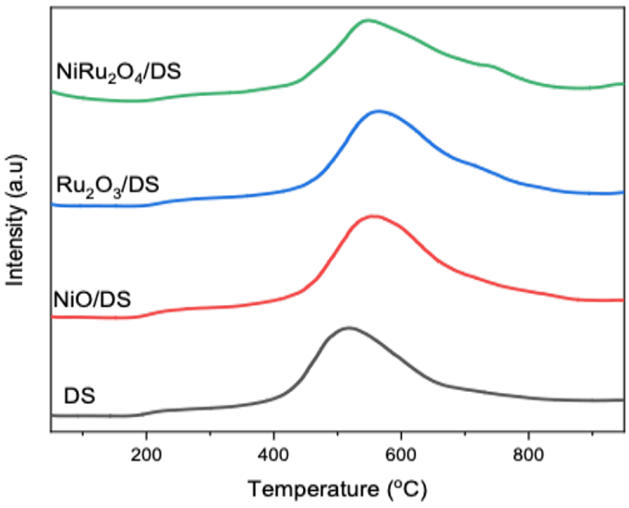

Figure 8. TPD-CO_2 profiles of the synthesized catalysts.

Table 4. Surface basicity and CO_2 desorption parameters of the synthesized catalysts.

Catalyst	CO_2- desorption temperature (°C)	Amount of CO_2- desorbed (µmol/g)
Date Seeds (DS)	518	6714.0
NiO/DS	555	5378.9
Ru_2O_3/DS	565	8334.1
$NiRu_2O_4$/DS	548	8534.6

3.2. Catalytic Deoxygenation Activity of New Catalysts

3.2.1. Gas Chromatography-Flame Ionization Detector (GC-FID) analysis

The catalytic efficiency of the synthesized materials was evaluated based on total hydrocarbon yield and selectivity toward kerosene and bio-jet fuel (BJF) components, as illustrated in Figure 10 (A-B). Within the investigated catalyst library, $NiRu_2O_4$/DS emerged as the most potent candidate, delivering a peak hydrocarbon yield of 95%, a kerosene-range selectivity of 83.33%, and a higher BJF selectivity of 43%, especially in C_{11} (Figure 10A). Consequently, the progression of both kerosene and BJF yields followed the ascending sequence: Ru_2O_3/DS < DS < NiO/DS < $NiRu_2O_4$/DS.

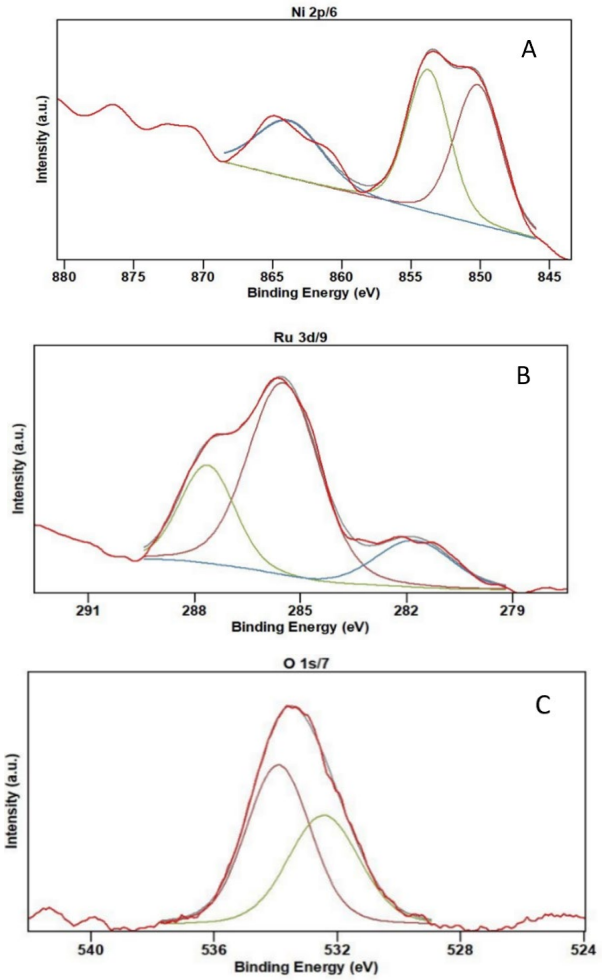

Figure 9. XPS spectra of the synthesized $NiRu_2O_4$ supported on date seeds (DS).

The superior catalytic performance of the NiRu/DS catalyst, as evidenced by the highest hydrocarbon (HC%) and kerosene yields, particularly in the C11 fraction, can be attributed to the synergistic effects of its physicochemical properties. The catalyst exhibited a moderate acidity of 2334 µmol/g and a relatively high basicity of 8534 µmol/g, providing a balanced distribution of active sites that promoted both deoxygenation and selective hydrocarbon formation. The acidic sites facilitated cracking, dehydration, and hydrocarbon chain rearrangement, whereas the abundant basic sites enhanced CO_2 adsorption and promoted deoxygenation pathways, thereby enabling more efficient oxygen removal from the feedstock. This balance between acidity and basicity minimized excessive cracking toward light gases while favoring the formation of liquid hydrocarbons in the kerosene range [30].

The enhanced deoxygenation performance can further be attributed to the synergistic interaction between NiO and Ru_2O_3. Based on the characterization results, the bimetallic catalyst exhibited higher acidity and basicity than the monometallic catalysts, indicating the generation of complementary active sites [30]. A possible electronic interaction between the two oxide phases may involve electron donation from Ru species to Ni species, producing electron-rich Ni sites and modifying the surface acid–base characteristics. In this system, NiO mainly

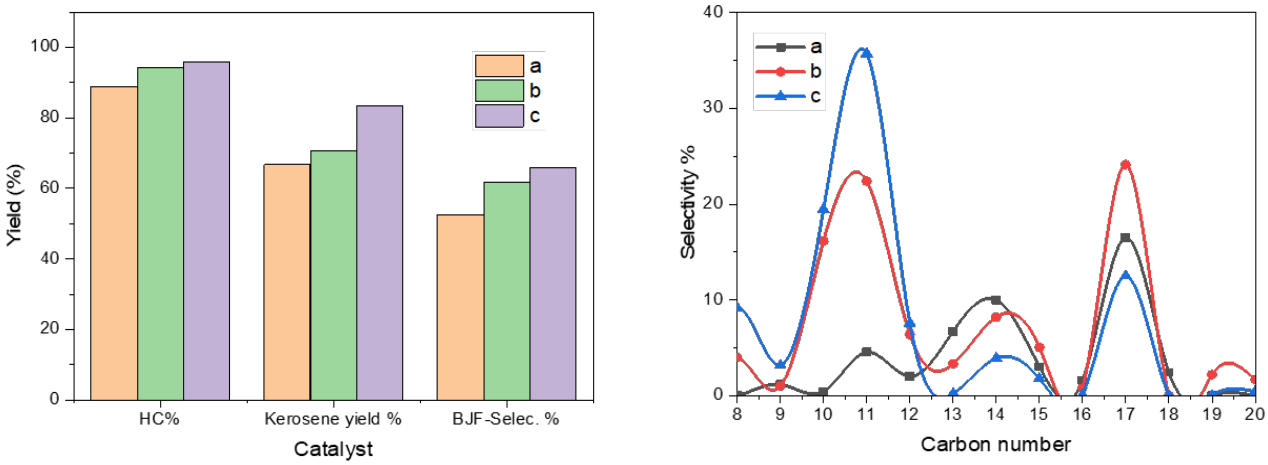

Figure 10. A) Kerosene yield, HC %, and BJF selectivity for a) DS, b) NiO/DS, c) $NiRu_2O_4$/DS, along with B) carbon selectivity of deoxygenated product.

provides acidic sites for the adsorption and activation of oxygenated intermediates, whereas Ru_2O_3 contributes basic sites that facilitate C-O bond cleavage and oxygen removal. The cooperation between these acidic and basic sites enhances decarboxylation and decarbonylation reactions while suppressing excessive cracking, thereby increasing hydrocarbon yield and improving selectivity toward kerosene-range products [31]. A schematic representation of the proposed catalytic mechanism is shown in Figure 11.

Although the catalyst possessed a relatively low BET surface area (4.4 m^2/g) and pore volume (0.0137 cm^3/g), its average pore diameter of 6.428 nm places it within the mesoporous range. These mesopores facilitated the diffusion of reactant molecules and reaction intermediates to the active sites, while reducing diffusion limitations. Therefore, catalytic activity was governed more by the nature and strength of the active sites than by the total surface area. All catalysts yielded high selectivity toward (C_{11} and C_{17}) hydrocarbons, as shown in Figure 10B. The formation of C_{17} hydrocarbons can be attributed to the decarboxylation and decarbonylation of C_{18} fatty acids, particularly oleic acid, which is one of the major components of palm oil which undergo a one-carbon loss alongside the elimination of oxygenated species to form C_{17} hydrocarbons. While the high kerosene selectivity, particularly toward C_{11} hydrocarbons, indicates that the catalyst provided an optimal balance between cracking and chain-growth reactions. Excessive acidity would have promoted over-cracking to lighter hydrocarbons, whereas the moderate acidity combined with strong basicity and the Ni–Ru synergistic effect favored the production of hydrocarbons within the kerosene boiling range [32-34].

Conversely, the Ru_2O_3/DS analog demonstrated minimal efficacy, yielding only 9%, attributable to its low surface area (1.9 m^2/g) and limited pore volume (0.00318 cm^3/g), which reduced the accessibility of active sites and hindered triglyceride diffusion within the pore channels. In addition, Ru particle agglomeration may have partially blocked the pores, resulting in lower catalytic activity and deoxygenation efficiency compared with the bimetallic catalyst.

Compared with previously reported DO catalysts, the synthesized $NiRu_2O_4$/DS catalyst exhibited markedly superior performance. The $Ni_{20}Zn_x$/AC catalyst achieved a hydrocarbon yield ranging from 77-83% [35]. The mesoporous 10%Ni-Fe/SBA-15 catalyst achieved the highest liquid hydrocarbon yield of 73.1% [36]. Similarly, the NiO-MoO_2/CeO_2 catalyst achieved an HC

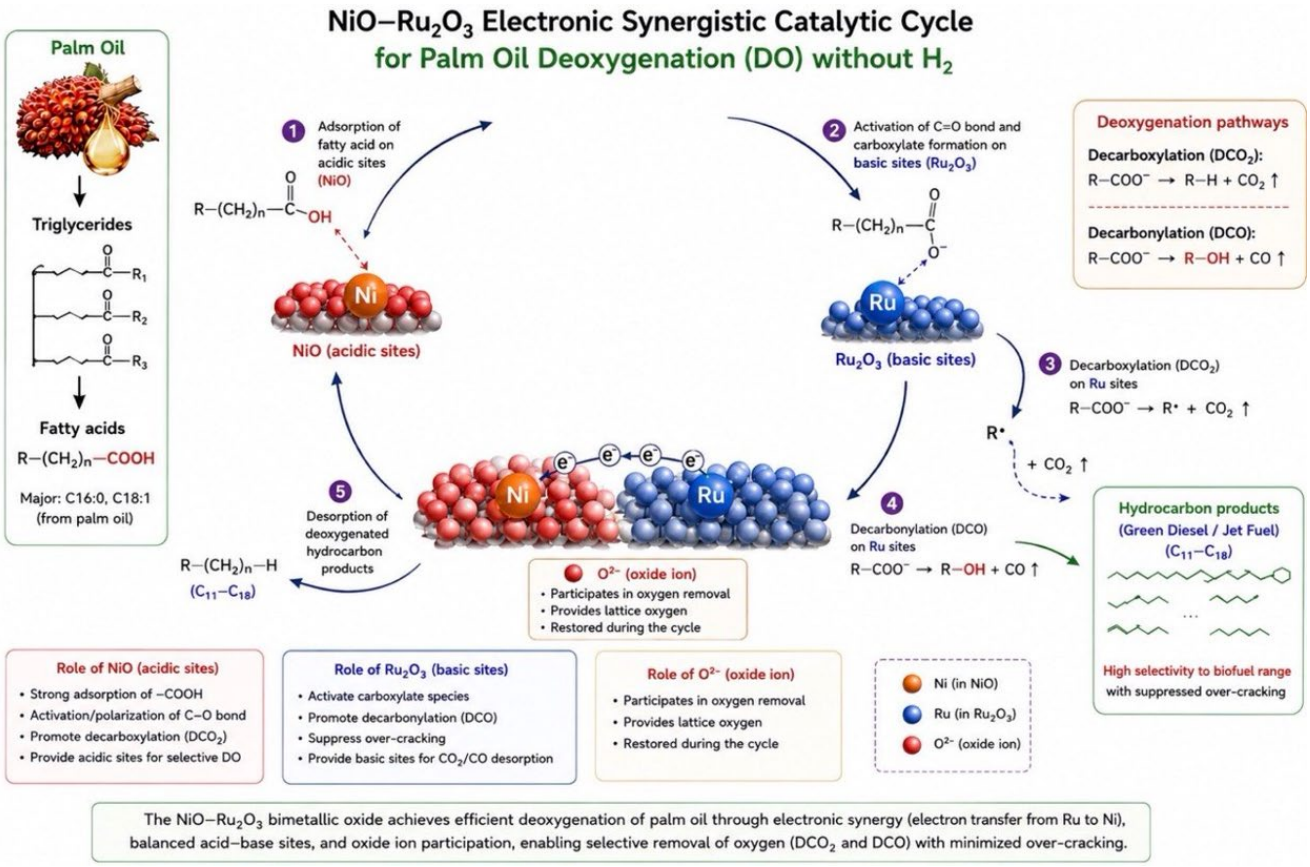

Figure 11. Proposed electronic synergistic catalytic mechanism of the NiO-Ru_2O_3/DS catalyst during palm oil deoxygenation.

yield of approximately 77% at a relatively high catalyst loading of 15 wt% and 300 °C [33]. In contrast, $NiRu_2O_4$/DS achieved a substantially higher HC yield (95%) using only 5 wt% loading. While Fe/AC showed only 55% HC yield and 52% alkane selectivity in palmitic acid DO at 450 °C [32], both were surpassed by $NiRu_2O_4$/DS at a lower temperature of 350 °C. The superior catalytic performance of the $NiRu_2O_4$/DS catalyst can be attributed to the synergistic interplay of its physicochemical characteristics. The catalyst exhibited a moderate acidity of 2334 µmol/g and a relatively high basicity of 8534 µmol/g, resulting in a well-balanced distribution of active sites that effectively facilitated deoxygenation reactions and promoted the selective formation of hydrocarbons.

Moreover, the incorporation of Ni and Ru created highly active metallic centers that promoted both hydrogenation and hydrogenolysis processes. The cooperative interaction between these metals facilitated the efficient transformation of oxygen-containing intermediates into stable hydrocarbon compounds, thereby enhancing overall hydrocarbon production.

3.2.2. Gas Chromatography-Mass Spectrometry (GC-MS)

The GC-MS analysis demonstrated the varying efficiencies of the modified catalysts in converting the feedstock into hydrocarbons, as shown in Figure 12. According to experimental data, the $NiRu_2O_4$/DS catalysts achieved a total yield of nearly 94%, exhibiting the most pronounced shift toward producing both alkanes and alkenes. Conversely, only small amounts of the remaining oxygenated compounds (including acids and ketones) were recorded, totaling 6%. The high selectivity for (C_{11} and C_{17}) hydrocarbons can be attributed to the balanced acidic-basic properties together with the synergistic effect of

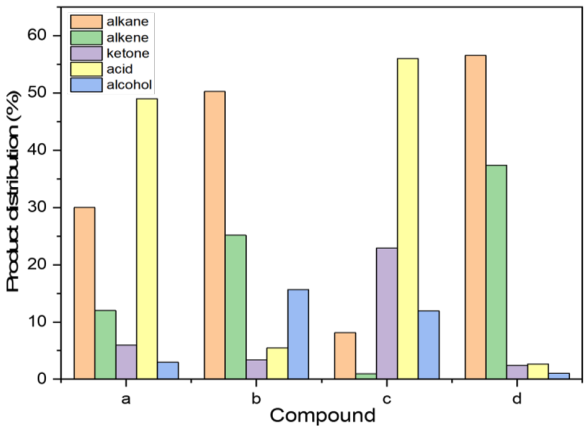

Figure 12. Distribution profile of liquid product obtained from the DO reaction for 3 h, at 350 °C and 5 wt% loading for a) DS, b) NiO/DS, c) Ru_2O^3/DS, d) $NiRu_2O_4$/DS.

active metal species. The high basicity promoted deoxygenation via DCO_2/DCO pathways, leading to the formation of long-chain hydrocarbons such as C_{17} [37,38]. At the same time, the presence of sufficient acidic sites facilitated controlled C-C bond cracking, resulting in the generation of lighter hydrocarbons within the BJF range, particularly C_{11}.

In contrast, the Ru_2O_3/DS catalyst exhibited opposite behavior, producing a total yield of only 9% hydrocarbons and the highest yield of oxygenated compounds, reaching 91%, particularly fatty acids, which accounted for 56.04% of the total composition, alongside alcohols and ketones, due to its poor textural properties compared with the bimetallic catalyst. In this case, the presence of ruthenium favored incomplete deoxygenation of intermediates rather than their complete conversion to fully saturated hydrocarbons.

3.2.3. Optimization studies and reusability

Using a one-variable-at-a-time (OVAT) approach, reaction parameters for the deoxygenation (DO) reaction were optimized with the $NiRu_2O_4$/DS catalyst. These include temperature (270-370 °C), catalyst loading (1, 3, 5, 10 wt%), and reaction time (2-6 h) under an N_2 Atmosphere at 400 rpm. Results showed that at lower temperatures, Incomplete deoxygenation occurred due to insufficient energy for effective C-O bond cleavage. In contrast, temperatures above 350 °C promoted excessive cracking, thereby decreasing selectivity toward diesel-range hydrocarbons. Likewise, increasing the catalyst loading beyond 5 wt% did not significantly enhance the product yield because higher solid concentrations limited mass transfer and promoted secondary cracking reactions. The optimal reaction conditions were 350 °C, 3 h, and a catalyst loading of 5 wt%. Under these conditions, the process yielded hydrocarbons at 95% with a selectivity towards Bio-jet fuel (BJF) of 43%. These conditions were used to determine the stability and reusability of the $NiRu_2O_4$/DS catalyst.

3.2.4. Reusability and stability of the optimal catalyst

The stability and reusability of the catalyst were investigated under previously optimized reaction conditions, including 350 °C, 3 h, and a catalyst loading of 5 wt%. After each reaction, the catalyst was separated by filtration, washed with n-hexane to remove organic byproducts and residues, dried, and reused. The catalyst was stable over three reaction cycles. However, hydrocarbon yield gradually declined, as shown by GC-FID analysis (Figure 13B), from 95.0% in the first cycle to 91.2% and 88.5% in the second

and third cycles, respectively. This decline is likely due to partial catalyst deactivation from carbon accumulation, pore blockage, or slight agglomeration of active sites. This behavior is frequently observed in heterogeneous catalysts at high temperatures, without substantially diminishing catalytic activity.

To investigate the catalyst's selectivity and product quality, GC-MS analysis was performed on the liquid product from each cycle. GC-MS analysis showed that hydrocarbons in the C_{14}-C_{17} range were the dominant products in all reaction cycles. Despite the slight decline in total hydrocarbon yield. This distribution is related to the fatty acid composition of palm oil, which is rich in C_{16} and C_{18} fatty acids. During deoxygenation, C_{18} fatty acids undergo DCO_2/DCO reactions to form C_{17} hydrocarbons, explaining the high selectivity toward C_{17}. Meanwhile, C_{14} hydrocarbons are likely produced through secondary cracking of longer-chain intermediates. The simultaneous formation of C_{14} and C_{17} indicates that both deoxygenation and cracking reactions occurred over the catalyst surface. Bio-jet fuel (BJF) selectivity was calculated according to Equation (4) using the relative peak areas of C_{11}, C_{13}, and C_{15} hydrocarbons, resulting in a BJF selectivity of 43%. The presence of these hydrocarbons reflects the catalyst's ability to convert palm oil into jet-fuel-range products through controlled chain-shortening reactions. As shown in Figure 13A, the most abundant products and similar chromatographic profiles across all cycles suggest that the selectivity of the $NiRu_2O_4$/DS catalyst toward bio-jet fuel-range hydrocarbons remained unchanged. This study demonstrates the catalyst's stable reusability and the quality of the product in green fuel production.

To evaluate potential catalyst deactivation, XRD measurements were performed on the spent catalyst. The XRD pattern of the spent catalyst is illustrated in Figure 14. The diffraction patterns show a broad peak between 20° and 30°, along with evidence of the amorphous carbon support derived from date seeds. Additionally, the sharp and more intense diffraction peaks seen at 37.5° (1 1 1), 52° (2 0 0), 65.3° (2 2 2), and 77.8° (3 1 1) planes indicate the presence of cubic NiO (ICDD 04-0787) [6]. The diffraction peak at 2θ = 44.5 ° (1 0 1) indicates the presence of hexagonal crystalline phases of (Ru_2O_3) (ICDD 00-002-1365). The preservation of the main diffraction peaks confirms that the catalyst framework remained relatively stable, while the slight increase in peak intensity may also suggest coke deposition or formation of secondary crystalline phases on the catalyst surface.

Analysis of the spent $NiRu_2O_4$/DS catalyst through TGA in Figure 15 revealed good thermal stability up to approximately 350 °C, with only a minor weight loss ~6 wt.% attributed to the removal of physically adsorbed moisture and volatile species. A pronounced weight loss step (~30–32 wt.%) occurred between approximately

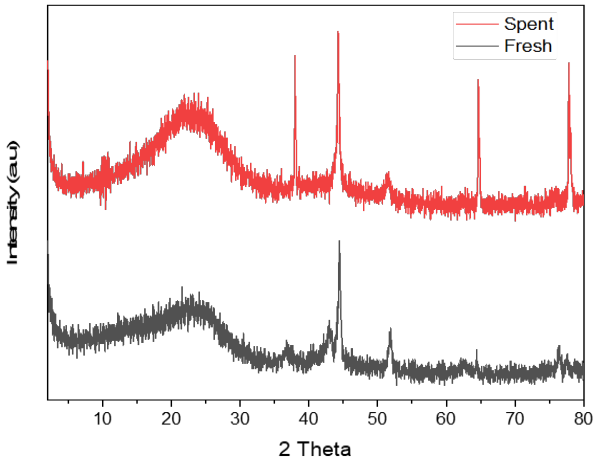

Figure 14. XRD patterns of the fresh and spent catalyst.

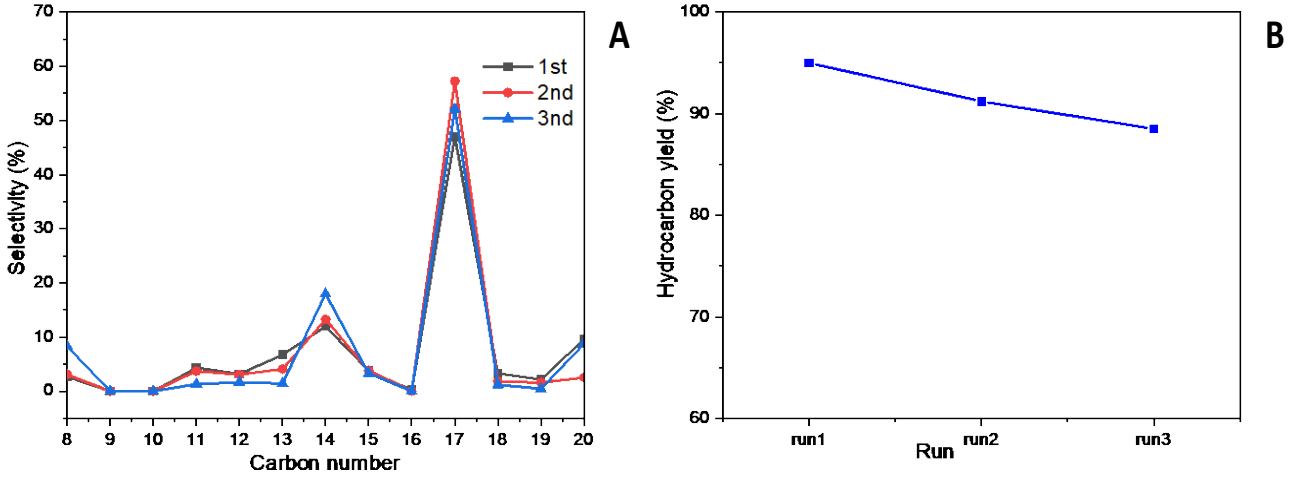

Figure 13. A) Carbon number distribution of product from the catalyst reusability study, B) Hydrocarbon yield over the 3rd run.

380 and 480 °C, corresponding to the combustion of carbonaceous deposits (coke) formed during the deoxygenation reaction. Beyond ~500 °C, the mass remained essentially constant up to 1000 °C, with a final residue of approximately 61–62 wt.%, associated with the remaining inorganic framework. In contrast, the fresh catalyst exhibited a gradual, multi-step weight loss across the entire temperature range (100-1000 °C), without the sharp single-stage decomposition seen in the spent sample, ultimately reaching a comparable residual mass (~60 wt.%). The distinct, sharp decomposition step observed only in the spent catalyst is attributed to the additional combustion of coke deposits accumulated during the reaction, providing direct evidence that carbonaceous deposition is a contributing deactivation pathway.

The TEM analysis of the used catalyst (Figure 16.B) shows that metal particle agglomeration reached a critical point due to a consistently high temperature of 350 °C. Increasing particle size explains the efficiency loss from 95% to 88%. Furthermore, an amorphous carbonaceous coke layer formed around the active sites because of deoxygenation pathways. This layer created a physical barrier that limited the reactants' ability to reach the metal. These changes were offset by the Date Stone (DS)-derived support, which exhibited high structural stability and strong support under high pressure, consistent with an increase in crystallite size observed in XRD and the weight loss observed in TGA.

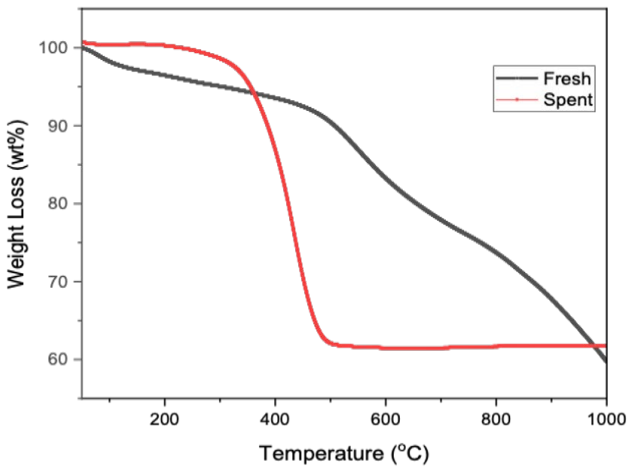

Figure 15. Thermogravimetric analysis (TGA) profiles for fresh and spent $NiRu_2O_4$/DS catalysts after catalytic reaction cycles.

4. Conclusion

The catalytic proficiency and structural robustness of the $NiRu_2O_4$/DS system were systematically examined during the deoxygenation of palm oil to synthesize bio-jet fuel. Under optimized experimental parameters (350 °C, 3 h, and 5 wt% catalyst loading), the initial catalytic trial achieved a peak hydrocarbon yield of 95%. Longevity assessments confirmed the catalyst's stability, with successive yields of 91% and 88% recorded over three cycles. Furthermore, GC-MS characterization revealed a high selectivity for C_{14} and C_{17} alkanes, meeting the stringent quality standards for high-grade aviation biofuels. Although a marginal decline in activity was observed, likely due to pore clogging or carbonaceous accumulation, the primary reaction pathways remained unaffected. Consequently, $NiRu_2O_4$/DS stands out as a technically sound and sustainable candidate for the industrial-scale production of renewable jet fuels.

Acknowledgment

Recognize those who helped in the research, especially funding source supporter (Funder of Research) of your research financially. Please read Author Guideline Section 11.19 (https://journal.bcrec.id/index.php/bcrec/pages/view/authorguide).

CRedit Author Statement

Author Contributions: please provide Credit Author Statement as guide in Author Guideline Section 11.13 (https://journal.bcrec.id/index.php/bcrec/pages/view/authorguide). All authors have read and agreed to the published version of the manuscript.

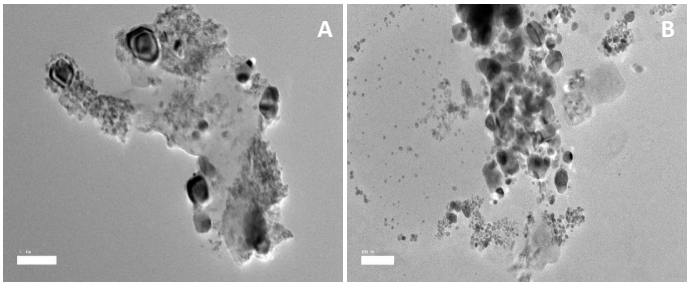

Figure 16. TEM micrograph of A) fresh catalyst and B) spent catalyst.

References

[1] Pratama, J., Rahmawati, Z., Widyanto, A., Gunawan, T., Wan Abdullah, W.N.L., Fansuri, H. (2024). Advancements in green diesel production for energy sustainability : a comprehensive bibliometric analysis. *RSC Adv*. 14, 36040–36062. DOI: 10.1039/d4ra06262k

[2] Asikin-Mijan, N., Juan, J.C., Taufiq-Yap, Y.H., Ong, H.C., Lin, Y.C., AbdulKareem-Alsultan, G., Lee, H. (2023). Towards sustainable green diesel fuel production : Advancements and opportunities in acid-base-catalyzed H_2-free deoxygenation process. *Catal. Commun.* 183, 106741. DOI: 10.1016/j.catcom.2023.106741.

[3] Hongloi, N., Prapainainar, P., Muadmai, T., Namboonlue, J., Seubsai, A., Prapainainar, C., (2021). Green Diesel Production from Oleic Acid Deoxygenation Using Subcritical Water under Hydrogen-Free Conditions. *Eng. J.* 25, 115–122. DOI: 10.4186/ej.2021.25.10.115.

[4] Chaudhry, B., Ahmad, M., Munir, Mamoona, Fawzy Ramadan, M., Munir, Mumna, Ussemane Mussagy, C., Faisal, S., Abdellatief, T.M.M., Mustafa, A., (2024). Unleashing the power of non-edible oil seeds of Ipomoea cairica for cleaner and sustainable biodiesel production using green Molybdenum Oxide (MoO_3) nano catalyst. *Sustain. Energy Technol. Assessments,* 65, 103781. DOI: 10.1016/j.seta.2024.103781.

[5] Rahmawati, Z., Santoso, L., Mccue, A., Azua, L. (2023). RSC Advances Selectivity of reaction pathways for green diesel production towards biojet fuel applications. *RSC Adv*. 13, 13698–13714. DOI: 10.1039/D3RA02281A.

[6] Hassn, A.F., Abdulsahib, H.T., Al-Doghachi, F.A.J., Yun Hin, T. (2026). Efficient Deoxygenation of Palm Oil to Green Diesel Using a Metal Oxide Catalyst Supported on ZrO2-Enhanced Graphene Oxide. *Bulletin of Chemical Reaction Engineering & Catalysis*, 21(3), 697-709. DOI: 10.9767/bcrec.20693.

[7] Aziz, I., Sugita, P., Darmawan, N., Adep, A., Dwiatmoko, A.A. (2023). Synthesis of green diesel from palm oil using a nickel-based catalyst: A review. *J. Kim. Val.* 9, 59-75. DOI: 10.15408/jkv.v9i1.26488.

[8] Nugraha, R.E., Sunarti, A.R.Y., Tehubijuluw, H., Mumtazah, Z. (2022). Effect of catalyst properties on the deoxygenation reaction of vegetable oil and model compound to produce diesel-range hydrocarbon fuels: A review. *J. Kim. Ris.* 7, 81–93. DOI: 10.20473/jkr.v7i1.35974.

[9] Rajak, A.K., Dalal, S., Harikrishna, M., Sahoo, U.K., Karuna, M.S.L., Sarangi, P.K. (2025). A comprehensive review of biomass-derived heterogeneous catalysts for efficient biodiesel production. *Asian J. Water, Environ. Pollut.* 22, 1–54. DOI: 10.36922/AJWEP025130095.

[10] Al-Doghachi, F.A.J., Rashid, U., Taufiq-Yap, Y.H. (2016). Investigation of Ce (III) promoter effects on the tri-metallic Pt, Pd, Ni/MgO catalyst in dry reforming of methane. *RSC Adv*. 6, 10372–10384. DOI: 10.1039/C5RA25869C.

[11] Naranov, E. (2024). Sustainable production of chemicals via hydrotreating of CO2 and biomass-derived molecules using heterogeneous noble metal oxide catalysts. *ChemCatChem* 16, e202301268. DOI: 10.1002/cctc.202301268.

[12] Alghamdi, H.S., Ali, A., Ajeebi, A.M., Jedidi, A., Sanhoob, M., Aktary, M., Shabi, A.H., Usman, M., Alghamdi, W., Alzahrani, S. (2024). Catalysts for liquid organic hydrogen carriers (LOHCs): efficient storage and transport for renewable energy. *Chem. Rec.* 24, e202400082. DOI: 10.1002/tcr.202400082.

[13] Adzahar, N.A., Abdulkareem-Alsultan, G., Mijan, N.A., Mastuli, M.S., Lee, H.V., Yun Hin T. (2026). Enhancing aviation sustainability : bimetallic Ni – Co catalysts for bio-jet fuel from palm kernel oil. *Fuel.* 405, 136388. DOI: 10.1016/j.fuel.2025.136388.

[14] Adzahar, N.A., AbdulKareem-Alsultan, G., Lee, H.V., Taufiq-Yap, Y.H., Lee, V., (2025). Advances in supported monometallic and bimetallic catalysts towards green aviation fuels: a review. *Energy Adv*. 4, 966-1005. DOI: 10.1039/D5YA00078E.

[15] Athirah, N., Abdulkareem-alsultan, G., Mijan, N.A., Mastuli, M.S., Lee, H. V, Taufiq-yap, Y.H., (2025). Effect of catalyst synthesis of bimetallic nickel-cobalt-supported iron-based catalysts on the conversion of palm kernel oil into bio-jet fuel via deoxygenation. *Energy,* 314, 133957. DOI: 10.1016/j.energy.2024.133957.

[16] Salam H.H. Al-Jaberia, Umer Rashid, Fairs A.J. Al-Doghachi, G. Abdulkareem-Alsultan (2017). Synthesis of MnO-NiO-SO_4^{-2}/ZrO_2 solid acid catalyst for methyl ester production from palm fatty acid distillate. *Energy Conversion and Management.* 139, 166-174. DOI: 10.10.16/j.enconman.2017.02.056

[17] Al-Zahrani, F.A.M., Al-Shehri, B.M., El-Shishtawy, R.M., Awwad, N.S., Khan, K.A., Sayed, M.A., Siddeeg, S.M. (2022). Characterization of date seed powder-derived porous graphene oxide and its application as an environmental functional material to remove dye from aqueous solutions. *Materials (Basel).* 15, 8136. DOI: 10.3390/ma15228136.

[18] Kim, H.B., Park, E.D. (2023) Ammonia decomposition over Ru catalysts supported on alumina with different crystalline phases. *Catalysis Today.* 411-412. DOI: 10.1016/j.cattod.2022.06.032.

[19] Geetha, N.B., Boopathy, S.S., Sindhuja, A., (2025). Fabrication and Analysis of Nickel Oxide Nanoparticles for Advanced Applications .*The Bioscan* 20, 621–625. DOI: 10.63001/tbs.2025.v20.i02.S2.pp621-625.

[20] Al-Doghachi, F.A., Al-Najar, A.M., Safa-Gamal, M., Taufiq-Yap, Y.H. (2023). Catalytic Dry Reforming of Methane Process with Co,Ni,Pd/Ca-La-O Mixed Oxides. *Bulletin of Chemical Reaction Engineering & Catalysis.* 18(4), 677. DOI: 10.9767/bcrec.20053.

[21] Pratama, J., Rahmawati, Z., Widyanto, A., Gunawan, T., Wan Abdullah, W.N.L., Fansuri, H. (2024). Advancements in green diesel production for energy sustainability : a comprehensive bibliometric analysis. *RSC Adv.* 14, 36040–36062. DOI: 10.1039/d4ra06262k

[22] Asikin-Mijan, N., Juan, J.C., Taufiq-Yap, Y.H., Ong, H.C., Lin, Y.C., AbdulKareem-Alsultan, G., Lee, H., (2023). Towards sustainable green diesel fuel production : Advancements and opportunities in acid-base-catalyzed H_2-free deoxygenation process. *Catal. Commun.* 183, 106741. DOI: 10.1016/j.catcom.2023.106741.

[23] Hongloi, N., Prapainainar, P., Muadmai, T., Namboonlue, J., Seubsai, A., Prapainainar, C., (2021). Green Diesel Production from Oleic Acid Deoxygenation Using Subcritical Water under Hydrogen-Free Conditions. *Eng. J.* 25, 115–122. DOI: 10.4186/ej.2021.25.10.115.

[24] Chaudhry, B., Ahmad, M., Munir, Mamoona, Fawzy Ramadan, M., Munir, Mumna, Ussemane Mussagy, C., Faisal, S., Abdellatief, T.M.M., Mustafa, A., (2024). Unleashing the power of non-edible oil seeds of Ipomoea cairica for cleaner and sustainable biodiesel production using green Molybdenum Oxide (MoO3) nano catalyst. *Sustain. Energy Technol. Assessments*, 65, 103781. DOI: 10.1016/j.seta.2024.103781.

[25] Rahmawati, Z., Santoso, L., Mccue, A., Azua, L. (2023). RSC Advances Selectivity of reaction pathways for green diesel production towards biojet fuel applications. *RSC Adv.* 13, 13698–13714. DOI: 10.1039/D3RA02281A.

[26] Hassn, A.F., Abdulsahib, H.T., Al-Doghachi, F.A.J., Yun Hin, T. (2026). Efficient Deoxygenation of Palm Oil to Green Diesel Using a *Metal* Oxide Catalyst Supported on ZrO2-Enhanced Graphene Oxide. *Bulletin of Chemical Reaction Engineering & Catalysis*, 21(3), 697-709. DOI: 10.9767/bcrec.20693.

[27] Aziz, I., Sugita, P., Darmawan, N., Adep, A., Dwiatmoko, A.A. (2023). Synthesis of green diesel from palm oil using a nickel-based catalyst: A review. *J. Kim. Val.* 9, 59-75. DOI: 10.15408/jkv.v9i1.26488.

[28] Nugraha, R.E., Sunarti, A.R.Y., Tehubijuluw, H., Mumtazah, Z. (2022). Effect of catalyst properties on the deoxygenation reaction of vegetable oil and model compound to produce diesel-range hydrocarbon fuels: A review. *J. Kim. Ris.* 7, 81–93. DOI: 10.20473/jkr.v7i1.35974.

[29] Rajak, A.K., Dalal, S., Harikrishna, M., Sahoo, U.K., Karuna, M.S.L., Sarangi, P.K. (2025). A comprehensive review of biomass-derived heterogeneous catalysts for efficient biodiesel production. *Asian J. Water, Environ. Pollut.* 22, 1–54. DOI: 10.36922/AJWEP025130095.

[30] Al-Doghachi, F.A.J., Rashid, U., Taufiq-Yap, Y.H. (2016). Investigation of Ce(III) promoter effects on the tri-metallic Pt, Pd, Ni/MgO catalyst in dry reforming of methane. *RSC Adv.* 6, 10372–10384. DOI: 10.1039/C5RA25869C.

[31] Naranov, E. (2024). Sustainable production of chemicals via hydrotreating of CO2 and biomass-derived molecules using heterogeneous noble metal oxide catalysts. *ChemCatChem*, 16, e202301268. DOI: 10.1002/cctc.202301268.

[32] Alghamdi, H.S., Ali, A., Ajeebi, A.M., Jedidi, A., Sanhoob, M., Aktary, M., Shabi, A.H., Usman, M., Alghamdi, W., Alzahrani, S. (2024). Catalysts for liquid organic hydrogen carriers (LOHCs): efficient storage and transport for renewable energy. *Chem. Rec.* 24, e202400082. DOI: 10.1002/tcr.202400082.

[33] Adzahar, N.A., Abdulkareem-Alsultan, G., Mijan, N.A., Mastuli, M.S., Lee, H.V., Yun Hin T. (2026). Enhancing aviation sustainability : bimetallic Ni – Co catalysts for bio-jet fuel from palm kernel oil. *Fuel*. 405, 136388. DOI: 10.1016/j.fuel.2025.136388.

[34] Adzahar, N.A., AbdulKareem-Alsultan, G., Lee, H.V., Taufiq-Yap, Y.H., Lee, V. (2025). Advances in supported monometallic and bimetallic catalysts towards green aviation fuels: a review. *Energy Adv.* 4, 966-1005. DOI: 10.1039/D5YA00078E.

[35] Athirah, N., Abdulkareem-alsultan, G., Mijan, N.A., Mastuli, M.S., Lee, H. V, Taufiq-yap, Y.H. (2025). Effect of catalyst synthesis of bimetallic nickel-cobalt-supported iron-based catalysts on the conversion of palm kernel oil into bio-jet fuel via deoxygenation. *Energy*, 314, 133957. DOI: 10.1016/j.energy.2024.133957.

[36] Al-Jaberia, S.H.H., Rashid, U., Al-Doghachi, F.A.J., Abdulkareem-Alsultan, G. (2017). Synthesis of MnO-NiO-SO4-2/ZrO2 solid acid catalyst for methyl ester production from palm fatty acid distillate. *Energy Conversion and Management.* 139, 166-174. DOI: 10.1016/j.fuel.2021.122695.

[37] Al-Zahrani, F.A.M., Al-Shehri, B.M., El-Shishtawy, R.M., Awwad, N.S., Khan, K.A., Sayed, M.A., Siddeeg, S.M. (2022). Characterization of date seed powder-derived porous graphene oxide and its application as an environmental functional material to remove dye from aqueous solutions. *Materials (Basel).* 15, 8136. DOI: 10.3390/ma15228136.

[38] Kim, H.B., Park, E.D. (2023) Ammonia decomposition over Ru catalysts supported on alumina with different crystalline phases. *Catalysis Today*. 411-412, 113817. DOI: 10.1016/j.cattod.2022.06.032.

[39] Geetha, N.B., Boopathy, S.S., Sindhuja, A. (2025). Fabrication and Analysis of Nickel Oxide Nanoparticles for Advanced Applications *The Bioscan*, 20, 621–625. DOI: 10.63001/tbs.2025.v20.i02.S2.pp621-625.

[40] Al-Doghachi, F.A., Al-Najar, A.M., Safa-Gamal, M., Taufiq-Yap, Y.H. (2023). Catalytic Dry Reforming of Methane Process with Co,Ni,Pd/Ca-La-O Mixed Oxides. *Bulletin of Chemical Reaction Engineering & Catalysis.* 18(4), 677. DOI: 10.9767/bcrec.20053.

[41] Neupane, S., Kaganas, G., Valenzuela, R., Kumari, L., Wang, X.W., Li, W.Z. (2011). Synthesis and characterization of ruthenium dioxide nanostructures. *J. Mater. Sci.* 46, 4803–4811. DOI: 10.1007/s10853-011-5390-2.

[42] Kishore, S.C., Perumal, S., Atchudan, R., Sundramoorthy, A.K., Alagan, R. (2022). A Review of Biomass-Derived Heterogeneous Catalysts for Biodiesel Production. *Catalysts*. 12, 1501. DOI: 10.3390/catal12121501.

[43] Alkhoori, S., Khaleel, M., Vega, L.F., Polychronopoulou, K. (2023). Deoxygenation of vegetable oils and fatty acids: How can we steer the reaction selectivity towards diesel range hydrocarbons. *J. Ind. Eng. Chem*. 127, 36–61. DOI: 10.1016/j.jiec.2023.07.031.

[44] Arias, S., González, J.F., Sousa, L. V, Barbosa, C.B.M., Silva, A.O.S., Frety, R., Pacheco, J.G.A. (2021). Influence of Ni/Al ratio on the fast pyrolysis of myristic acid when adsorbed on unsupported mixed oxides derived from layered double hydroxides. *Catal. Today*, 381, 181-191. DOI: 10.1016/j.cattod.2020.07.028.

[45] Wierzbicki, D., Debek, R., Motak, M., Grzybek, T., Gálvez, M.E., Da Costa, P. (2016). Novel Ni-La-hydrotalcite-derived catalysts for CO2 methanation. *Catal. Commun.* 83, 5–8. DOI: 10.1016/j.catcom.2016.04.021.

[46] Kuhaudomlap, S., Srifa, A., Koo-Amornpattana, W., Fukuhara, C., Ratchahat, S. (2024). Insight and comprehensive study of Ni-based catalysts supported on various metal oxides for CO2 methanation. *Scientific Reports*. 14, 23149. DOI: 10.1038/s41598-024-73848-0.

[47] Bustinza, A., Frías, M., Liu, Y., and García-Bordejé, E. (2020). Mono- and bimetallic metal catalysts based on Ni and Ru supported on alumina-coated monoliths for CO2 methanation. *Catal. Sci. Technol.* 10(12), 4061-4071. DOI: 10.1039/d0cy00639d.

[48] Al-Doghachi, F.A.J., Islam, A., Zainal, Z., Saiman, M.I., Embong, Z., Taufiq-Yap, Y.H. (2016). High Coke-Resistance Pt/Mg1-xNixO Catalyst for Dry Reforming of Methane. *PLOS One*, 11, e0145862. DOI: 10.1371/journal.pone.0145862.

[49] Zhang, Z., Zhao, G., Bi, G., Guo, Y., Xie, J. (2021). Monolithic SiC-foam-supported Ni-La2O3 composites for dry reforming of methane with enhanced carbon resistance. *Fuel Process. Technol.,* 212. DOI: 10.1016/j.fuproc.2020.106627.

[50] Guerero-Corona, C.E., Melo-Banda, J.A., Lam-Maldonado, M., Vega-Ibarra, L.A., Diaz-Zavala N.P., Meraz-Mel, M.A. (2024). Transition-metal oxide nanocatalysts for the deoxygenation of palm oil to green diesel. *Front. Chem. Eng*., 6. DOI: 10.3389/fceng.2024.1334355.

[51] Lakhani, P., Praikaew, W., Sukkasem, T., Assabumrungrat, S., Srifa, A. (2026). Simultaneous Deoxygenation and Isomerization for Environmentally Sustainable Biofuel Production: A Review of Bifunctional Ni-Based Catalysts. Advanced Energy and Sustainability Research, 7e70105. DOI: 10.1002/aesr.70195.

[52] Zulkepli, S., Lee, H.V., Rahman, N.A., Chuan, L.T., Show, P.L., Chen, W.-H., Juan, J.C. (2022). Highly active iron-promoted hexagonal mesoporous silica (HMS) for the deoxygenation of triglycerides to green hydrocarbon-like biofuel. *Fuel*. 308, 121860. DOI: 10.1016/j.fuel.2021.121860.

[53] Bian, Z., Das, S., Wai, M.H., Hongmanorom, P., Kawi, S. (2017). A Review on Bimetallic Nickel-Based Catalysts for CO2 Reforming of Methane. *ChemPhysChem,* 18, 3117–3134. DOI: 10.1002/cphc.201700529.

[54] Bian, J., Wang, Y., Zhang, Q., Fang, X., Feng, L., Li, C. (2017). Fatty acid decarboxylation reaction kinetics and pathway of co-conversion with amino acid on supported iron oxide catalysts. *RSC Adv*. 7, 47279-47287. DOI: 10.1039/C7RA08507A.

[55] Khalit, W.N.A.W., Asikin-Mijan, N., Marliza, T.S., Gamal, M.S., Shamsuddin, M.R., Saiman, M.I., Taufiq-Yap, Y.H. (2021). Catalytic deoxygenation of waste cooking oil utilizing nickel oxide catalysts over various supports to produce renewable diesel fuel. *Biomass and Bioenergy*, 154, 106248. DOI: 10.1016/j.biombioe.2021.106248.

[56] Rashidi, N.A., Mustapha, E., Theng, Y.Y., Razak, N.A.A., Bar, N.A., Baharudin, K.B., Derawi, D. (2022). Advanced biofuels from waste cooking oil via solventless and hydrogen-free catalytic deoxygenation over mesostructured Ni-Co/SBA-15, Ni-Fe/SBA-15, and Co-Fe/SBA-15 catalysts. *Fuel*. 313, 122695. DOI: 10.1016/j.fuel.2021.122695.

[57] Hart, A., Patel, H., Yildirir, E., Onwudili, J.A. (2025). Influence of surface acidity/basicity of selected metal oxide catalysts and reaction atmospheres on the ketonization of propionic acid to produce 3-pentanone as a liquid biofuel precursor. *Renew. Energy*. 250, 123386. DOI: 10.1016/j.renene.2025.123386.

[58] Zhou, L., Yang, H., Hu, C. (2025). Catalytic Deoxygenation of Lipids for Bio-Jet Fuel: Advances in Catalyst Design and Reaction Pathways. *Catalysts*. 15, 518. DOI: 10.3390/catal15060518.